Human Molecular Genetics, 2015, Vol. 24, No. 1 **76–85**
doi:10.1093/hmg/ddu421
Advance Access published on August 20, 2014

Mutant huntingtin alters Tau phosphorylation and subcellular distribution

David Blum[1,2,3,*], Federico Herrera[4,†], Laetitia Francelle[6,7,†], Tiago Mendes[4,*], Marie Basquin[1,2], Hélène Obriot[1,2], Dominique Demeyer[1,2], Nicolas Sergeant[1,2,3], Ellen Gerhardt[5], Emmanuel Brouillet[6,7], Luc Buée[1,2,3] and Tiago F. Outeiro[4,5]

[1]Université Lille-Nord de France, UDSL, F-59000, Lille, France, [2]Inserm U837, Jean-Pierre Aubert Research Centre, IMPRT, F-59000, Lille, France, [3]CHRU, F-59000, Lille, France, [4]Cell and Molecular Neuroscience Unit, Instituto de Medicina Molecular, Av. Prof. Egas Moniz, 1649-029 Lisboa, Portugal, [5]Department of Neurodegeneration and Restorative Research, Center for Nanoscale Microscopy and Molecular Physiology of the Brain, University Medical Center Goettingen, Waldweg 33, 37073 Goettingen, Germany, [6]CEA, DSV, I[2]BM, Molecular Imaging Research Center (MIRCen), Fontenay-aux-Roses F-92265, France and [7]CNRS, CEA URA 2210, Fontenay-aux-Roses F-92265, France

Received July 16, 2014; Revised and Accepted August 14, 2014

Tau abnormalities play a central role in several neurodegenerative diseases, collectively known as tauopathies. In the present study, we examined whether mutant huntingtin (mHtt), which causes Huntington's disease (HD), modifies Tau phosphorylation and subcellular localization using cell and mouse HD models. Initially, we used novel bimolecular fluorescence complementation assays in live cells to evaluate Tau interactions with either wild type (25QHtt) or mutant huntingtin (103QHtt). While 25QHtt and Tau interacted at the level of the microtubule network, 103QHtt and Tau interacted and formed 'ring-like' inclusions localized in the vicinity of the microtubular organizing center (MTOC). Fluorescence recovery after photobleaching experiments also indicated that, whereas homomeric 103QHtt/103QHtt pairs rapidly re-entered into inclusions, heteromeric 103QHtt/Tau pairs remained excluded from the 'ring-like' inclusions. Interestingly, *in vitro* Tau relocalization was associated to Tau hyperphosphorylation. Consistent with this observation, we found strong Tau hyperphosphorylation in brain samples from two different mouse models of HD, R6/2 and 140CAG knock-in. This was associated with a significant reduction in the levels of Tau phosphatases (PP1, PP2A and PP2B), with no apparent involvement of major Tau kinases. Thus, the present study strongly suggests that expression of mHtt leads to Tau hyperphosphorylation, relocalization and sequestration through direct protein–protein interactions in inclusion-like compartments in the vicinity of the MTOC. Likewise, our data also suggest that Tau alterations may also contribute to HD pathogenesis.

INTRODUCTION

Huntington's disease (HD) is an autosomal dominant inherited neurodegenerative disorder caused by mutations in the *IT15/HD1* gene that encodes huntingtin (Htt) protein (1). The mutation consists in a CAG triplet repeat expansion that is translated into an abnormally long polyglutamine (polyQ) tract (>39) within the N-terminal region of the protein (2). Mutant huntingtin (mHtt) leads to several neuronal and glial alterations, including notable transcriptional, mitochondrial and axonal transport defects, ultimately leading to neuronal death, primarily in striatal and cortical areas (3).

Tau is a microtubule-associated protein widely expressed in the central nervous system, playing a role in microtubule stabilization and axonal transport (4), synaptic plasticity (5) and neuronal response to stress (6). Tau hyperphosphorylation and aggregation are hallmarks of several neurodegenerative disorders referred to as Tauopathies, among which Alzheimer's

*To whom correspondence should be addressed at: Inserm U837, 'Alzheimer & Tauopathies', Place de Verdun, 59045, Lille Cedex, France. Tel: +33320298858; Fax: +33320538562; Email: david.blum@inserm.fr (D.B.); Department of Neurodegeneration and Restorative Research University Medical Center Goettingen, Waldweg 33, 37073 Goettingen, Germany. Tel: +495513913544; Email: touteiro@gmail.com (T.F.O.)
†These authors equally contributed to this work.

disease (AD) is included (7). Besides Tauopathies, Tau hyperphosphorylation has been associated with detrimental metabolic conditions as obesity and diabetes (8–11) but also impaired memory function due to chronic anesthesia (12,13).

The composition and location of protein aggregates are frequently used to diagnose and define neurodegenerative disorders. There is general consensus, for example, that α-synuclein is the main component of Parkinson's disease Lewy bodies, Tau and β-amyloid aggregate in AD, while mHtt aggregates in HD. However, α-synuclein interacts with Tau and also with Htt, possibly contributing to Alzheimer's or Huntington's pathologies, respectively (14–17). Notably, we showed that α-synuclein modifies the pattern of mHtt aggregation (18). Whether Htt mutation impacts upon Tau remains unknown so far. Previous data reported limited AD neuropathology in the brain of HD patients (19) and we reported co-aggregation of Htt and Tau in a patient exhibiting both corticobasal degeneration and huntingtin mutation (20). Altogether, these observations prompted us to evaluate the impact of mHtt upon Tau using both *in vitro* and *in vivo* HD models.

RESULTS

Tau hyperphosphorylation in HD mice

Initially, we evaluated Tau phosphorylation in two distinct HD mouse models, namely R6/2 and KI140. Given the important number of phosphorylation sites on Tau (>80; 4), we first performed a two-dimensional (2D) gel electrophoresis analysis to evaluate global changes in murine Tau protein in the cortex of HD mice. Upon membranes probing with a total Tau antibody (C-ter), we observed a significant shift of murine Tau isovariants from the basic to the acidic pH range in the cortex of R6/2 mice and KI140 (arrows, Fig. 1A and B) when compared with littermate controls, consistent with increased phosphorylation. This observation was in line with the shift of Tau isovariant following probing of 2D membranes with antibodies raised against

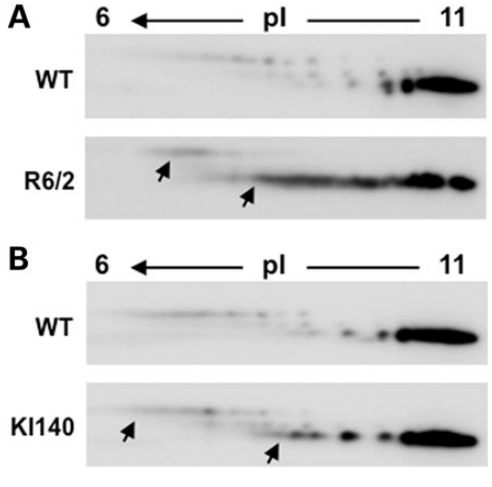

Figure 1. Global Tau phosphorylation in HD mice using Total Tau antibody. Comparison of representative two-dimensional profile of murine tau in the cortex of 10 week-old R6/2 (**A**) and 17 month-old KI140 (**B**) mice when compared with respective littermate controls. Profiles show increased Tau acidification in HD animals (arrows). The pH gradient used to resolve Tau protein is indicated at the top of 2D-western blots.

pSer404 and pSer396 (Supplementary Material, Fig. S1). Next, to confirm the occurrence of increased phosphorylation, we also performed SDS–PAGE and immunoblot analyses. In line with the 2D results, we found a significant increase in Tau phosphorylation at Ser396 and Ser404 in the cortex of R6/2 mice (Fig. 2A), while Tau-1 immunoreactivity representing unphosphorylated Tau was significantly decreased. In addition, we observed a significant shift of total Tau immunoreactive bands toward a higher apparent molecular weight (Fig. 2A). Similar changes were found in the cortex of KI140 animals (Fig. 2B) as well as in the striatum of both transgenic strains (Supplementary Material, Fig. S2). Increased phosphorylation at Ser396 was further confirmed using immunofluorescence analysis. Notably, the number of pSer396-Tau positive cells was increased in the brain of KI140 mice as shown in Supplementary Material, Figure S3.

In order to determine whether mHtt and Tau could interact, co-localize and eventually co-aggregate *in vivo*, we performed additional immunohistochemical and biochemical evaluations. Using confocal microscopy, we analyzed the expression of the two proteins in the brain of KI140 and littermate controls following immunofluorescence detection of Tau pSer396 and Htt (2B4 or Em48 antibodies). Results showed no major colocalization of the two proteins (Fig. 3). Lack of major *in vivo* interaction between Tau and Htt in the cortex HD animals was confirmed by co-immunoprecipitation studies (not shown). Finally, we failed to demonstrate the presence of Tau in cortical sarkosyl-insoluble protein fractions from R6/2 mice (Supplementary Material, Fig. S4).

Tau phosphorylation is under the tight control of several protein kinases and phosphatases (4). Here, we assessed the effects of mHtt on the expression or activation of major Tau protein kinases, such as GSK3β, CaMKII, Erk or cdk5. As shown in Figure 4A, neither expression nor activation of these kinases was found increased in R6/2 mice. Rather, we observed an increased Ser9 phosphorylation of GSK3β, reduced phosphorylation of CaMKII and reduced cdk5 expression in the cortex of R6/2 mice compared with littermate controls (Fig. 4A). Changes in CaMKII and cdk5 were also observed in the cortex of KI140 animals (Fig. 4B). These kinase changes thus fail to explain the increased Tau phosphorylation (Figs 1 and 2). In order to uncover a possible mechanism underlying Tau hyperphosphorylation in HD animals, we next assessed the expression levels of Tau protein phosphatases namely PP1, PP2A and PP2B (21). In R6/2 mice, we found an association of Tau hyperphosphorylation with a significant decrease in PP1, PP2A and PP2B expression (Fig. 4A). A trend for PP1 loss and a significant reduction in PP2B expression were also observed in KI140 animals (Fig. 4B). These results thus suggest that phosphatase dysregulation correlates with Tau phosphorylation changes in HD animals.

In vitro interaction between huntingtin and Tau

In a second series of experiments, we used an *in vitro* system to estimate the impact of mHtt on Tau phosphorylation and behavior and to evaluate a potential relationship between both proteins. We found that, as in the *in vivo* situation, mHtt expression promoted Tau hyperphosphorylation at S396 (Fig. 5B). Interestingly, using filter trap assays, we also observed that Tau inhibited 103QHtt aggregation (Fig. 5A). Wild type 25QHtt did not

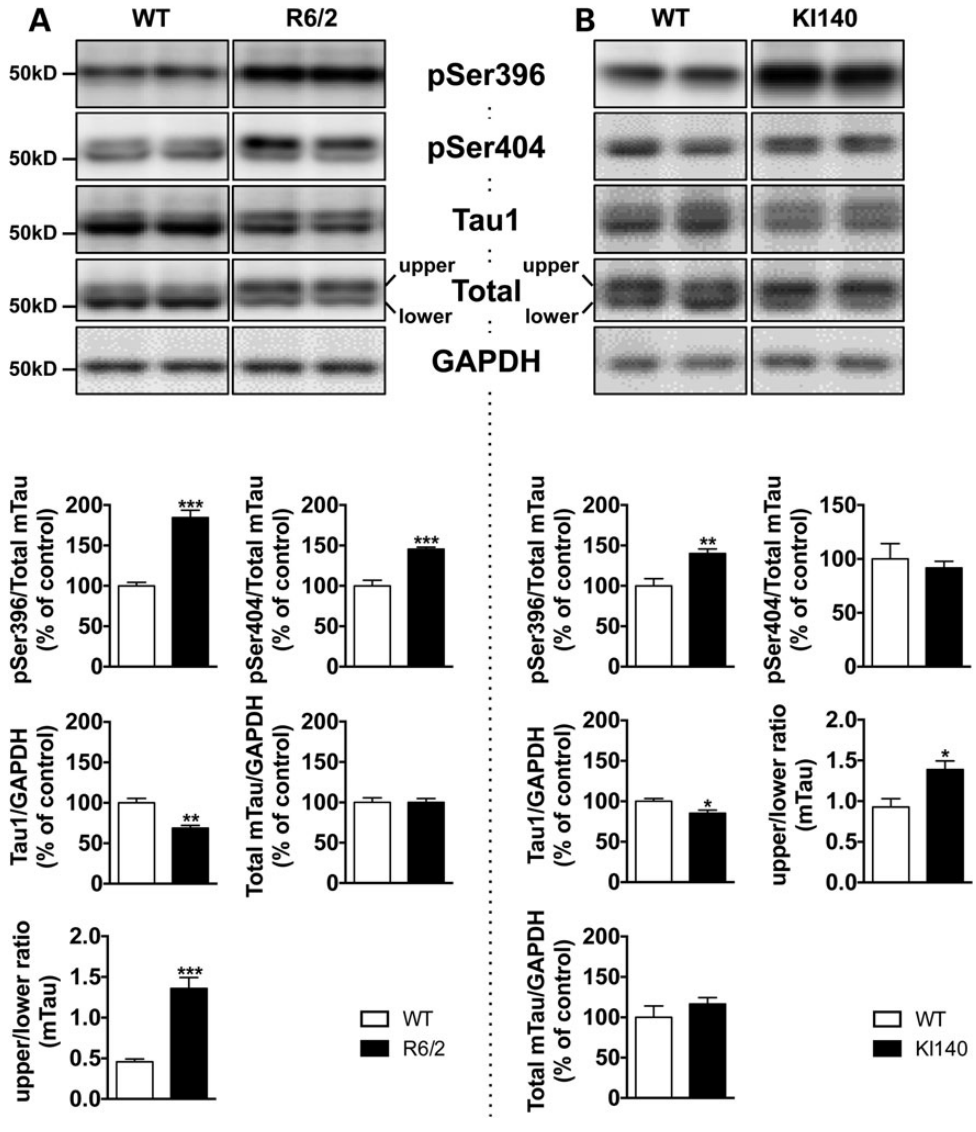

Figure 2. Immunoblot analysis of Tau phosphorylation in the cortex of HD mice. Analysis of Tau in the cortex of 10 week-old R6/2 (**A**) and 17 month-old KI140 (**B**) animals using antibodies targeting pSer396, pSer404, dephosphorylated Tau (Tau1) and Total Tau antibody (Cter). Quantifications indicate a significant enhancement of Tau phosphorylation at Ser396 and Ser404, a decreased dephosphorylated Tau using Tau1 antibody and a significant shift of Total Tau (Cter) immunoreactive bands toward a higher apparent molecular weight. Quantifications of phosphoepitopes were performed versus total Tau. Total Tau quantification was performed versus GAPDH. $^{*}P < 0.05$, $^{**}P < 0.01$, $^{***}P < 0.001$ versus littermate control using Student's *t*-test. $n = 5–6$/group.

produce SDS-insoluble aggregates in the presence or absence of Tau, while mutant 103QHtt produced more SDS-insoluble aggregates in the absence of Tau. Tau was retained in filter traps when it was co-expressed with 103QHtt, but not with 25QHtt, further indicating that mHtt and Tau co-aggregate *in vitro*. Interestingly, retained Tau was phosphorylated at S396.

In order to further evaluate the possible interaction between Htt and Tau at a cellular level, we used the bimolecular fluorescence complementation (BiFC) assay. In BiFC assays, the proteins of interest are fused to two non-fluorescent halves of a fluorescent reporter protein. When the proteins of interest dimerize/oligomerize, the two reporter halves are brought together and reconstitute the fluorophore, emitting fluorescence. Fluorescence is therefore indicative of dimerization/oligomerization. We have recently developed BiFC constructs for wild type (25Q) and mutant (103Q) Htt (22), as well as for Tau (Fig. 6A). Different combinations of 25QHtt, 103QHtt and Tau formed dimers/oligomers in human cells (Fig. 6B–G). Wild-type Htt BiFC pairs showed mostly a diffuse cytoplasmic fluorescence, indicative of the formation of dimers/oligomers (Fig. 6D), while 103QHtt BiFC pairs showed the occurrence of inclusion bodies (Fig. 6F). Tau/Tau BiFC pairs marked the microtubular network, as expected given the microtubule-binding properties of Tau (Fig. 6C and H). When 25QHtt was combined with Tau, the cellular phenotype resembled that of Tau BiFC pairs, indicating that Tau recruited 25QHtt to the microtubular network (Fig. 6E). On the other hand, combinations of 103QHtt with Tau produced a mixed phenotype. As with 25QHtt, 103QHtt was also recruited to the microtubular network, with all cells showing the microtubular cytoskeleton

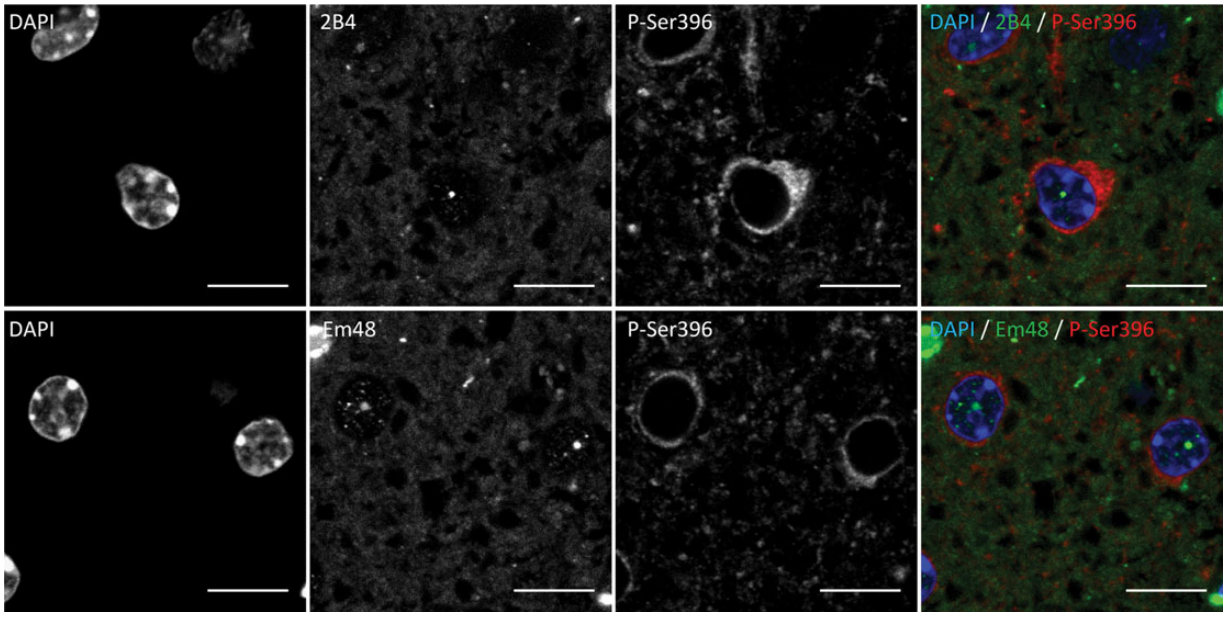

Figure 3. Absence of colocalization of pSer396 Tau and mHtt in the brain of KI140 HD mice. Confocal immunofluorescence images showing mutant Htt-containing intranuclear inclusions seen as typical round small dots in the nucleus (2B4, upper images; EM48, lower images) in the striatum of Ki140 mice. Immunofluorescence corresponding to Tau pSer369 (red) is mainly detected in the cytoplasm. No major colocalization of mutant Htt inclusions and Tau pSer396 was found. Similar results were obtained in three KI140 mice. Scale bar, 10 μm.

but, in addition, we also observed cells with large inclusions (Fig. 6G). None had the typical bright foci that characterize 103QHtt BiFC pairs (Fig. 6F). Notably, 103QHtt/Tau transfected cells often exhibited bright 'knot-like' inclusions in their microtubular cytoskeletons, close to where the microtubular organizing center (MTOC) is located (Fig. 6I). Besides BiFC experiments, we also evaluated whether mutant mHtt and Tau could colocalize in HEK293T cells following co-expression of c-myc tagged Htt171-82Q and non-tagged Tau. Confocal analysis showed that in a small proportion of transfected cells mHtt and phospho-Tau (AT8) colocalized in a perinuclear region compatible with MTOC (Supplementary Material, Fig. S5). These results are consistent with previous evidence showing that Htt binds to microtubules and localizes in the centrosome (23) and the mitotic spindle (24,25).

Mutant 103QHtt BiFC pairs characteristically produce aggregates in 30–40% of transfected cells (18,22) with an average of 14.70% (± 5.66) aggregates per cell (Fig. 6J). 103QHtt/Tau BiFC pairs produced 'knots' in 16.21% (± 1.27) of transfected cells. These 'knots' are larger than average 103QHtt aggregates, but are only one or two per cell (Fig. 6F versus G and J). A closer look to aggregates showed that most 103QHtt aggregates are solid (see Supplementary Material, Fig. S6), while 103QHtt/Tau aggregates had ring-like shape in their focal center, suggesting that they are hollow inclusions or complex rings (Supplementary Material, Fig. S7A; see also Supplementary Material, Figs S8 and S9 for full Z-stack videos). Furthermore, the dynamics of 103QHtt and 103QHtt/Tau aggregates, as well as of Tau dimers, were radically different (Supplementary Material, Fig. S7B and C). 103QHtt aggregates recovered relatively quickly after photobleaching (FRAP), indicating that they recruit new 103QHtt molecules to their core. The same was observed with Tau dimers, either at the MTOC or at the microtubules (Supplementary Material, Fig. S7D). On the other hand, 103QHtt/Tau aggregates did not recover after 2.5 min of monitoring (see also Supplementary Material, Figs S10 and 11 for full FRAP videos).

In summary, our *in vitro* results indicate that mHtt can interact with Tau and that this interaction interferes with the normal pattern of mHtt aggregation, favors Tau hyperphosphorylation and alters the subcellular distribution of Tau, promoting its aggregation.

DISCUSSION

The present study reports that expression of mHtt impacts on Tau cellular localization, molecular interactions and phosphorylation pattern. Strikingly, *in vitro*, Tau was found also able to modulate Htt aggregation. These results notably support a mutual relationship between mHtt and Tau proteins that might contribute to the neurodegenerative phenotype in HD.

Brain of symptomatic HD animals and cultured cells co-expressing mHtt and Tau constructs showed significant Tau hyperphosphorylation, indicating that the expression of the former is sufficient to promote hyperphosphorylation of the latter. Notably, in HD mice, we did not notice increase in the activity of the main Tau kinases. Rather, we found a congruent reduction of CaMKII and cdk5 expression in both R6/2 and KI140 mice. Reduced CamKII expression may notably rely on a reorganization of postsynaptic density as previously described (26). On the other hand, we observed significant phosphatase changes in HD lines. Both R6/2 and KI140 animals exhibited significant reduction of cortical PP2B expression, in line with previous observations in the brain of HD patients (27) and several HD models (28–30). PP2B dephosphorylates Tau at multiple

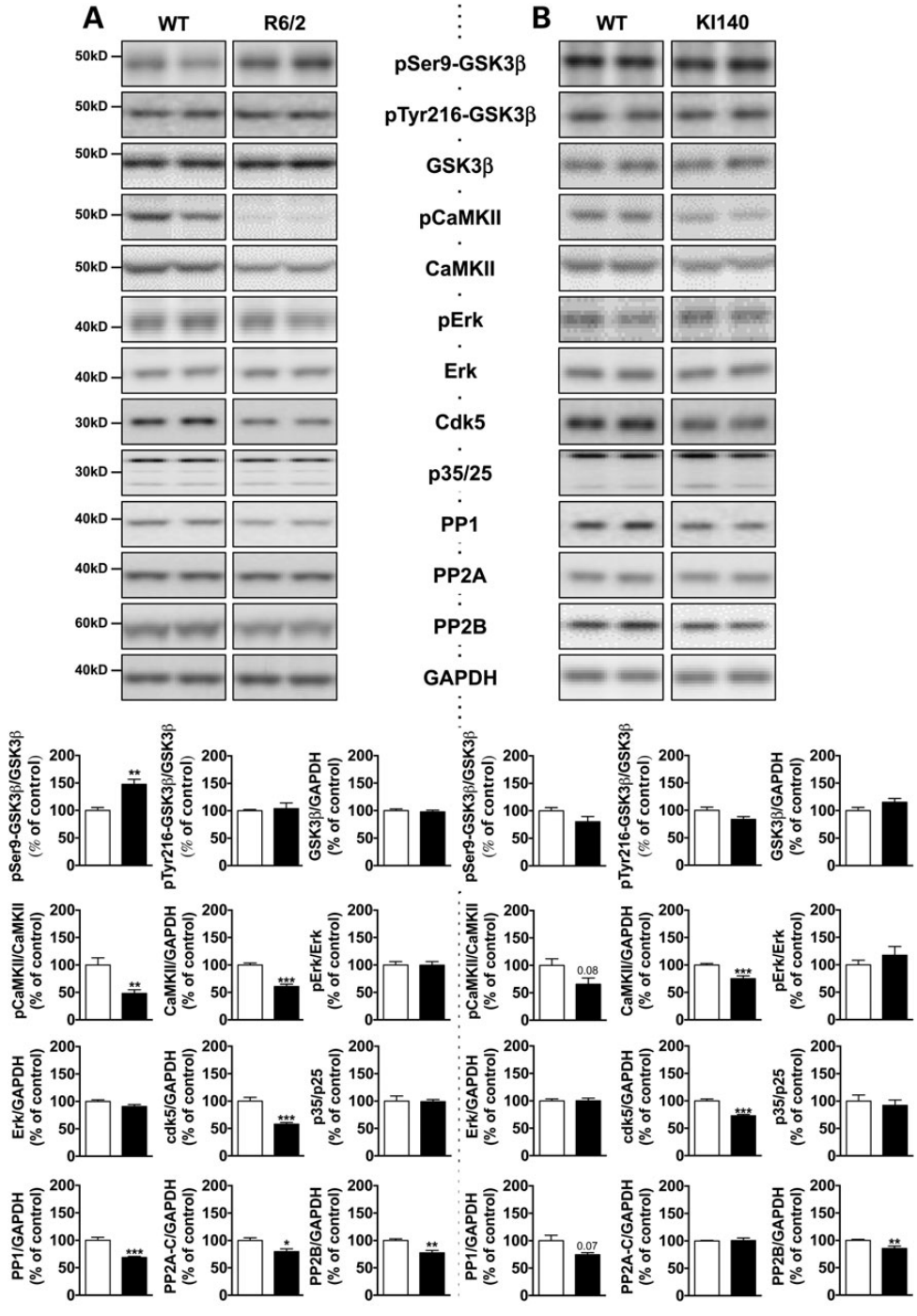

Figure 4. Tau kinases and phosphatases in HD mice. SDS–PAGE and immunoblot analysis was performed in the cortex of 10 week-old R6/2 (**A**) and 17 month-old KI140 (**B**) using antibodies raised against total and phosphorylated forms of several Tau kinases as well as phosphatases. Quantifications of phosphoepitopes were performed versus respective total protein. In other cases quantifications were performed versus GAPDH. $^{*}P < 0.05$, $^{**}P < 0.01$, $^{***}P < 0.001$ versus littermate control using Student's *t*-test. $n = 5–6$/group.

epitopes including those evaluated here (31). Therefore, a reduced PP2B expression is one possible explanation for increased Tau phosphorylation in transgenic HD mice and in cells expressing 103QHtt.

Our data indicate that expression of mHtt is associated with changes in Tau function. Indeed our *in vitro* data suggest that in addition to impact Tau hyperphosphorylation, mHtt leads to changes in its cellular distribution. Tau hyperphosphorylation is thought to impair its cellular localization (32) and its microtubule-stabilizing function (33). These observations suggest that HD would be associated with a loss of Tau function, at least regarding axonal transport, possibly contributing to the axonal transport defects previously reported in HD conditions (34). As Tau hyperphosphorylation can be associated with

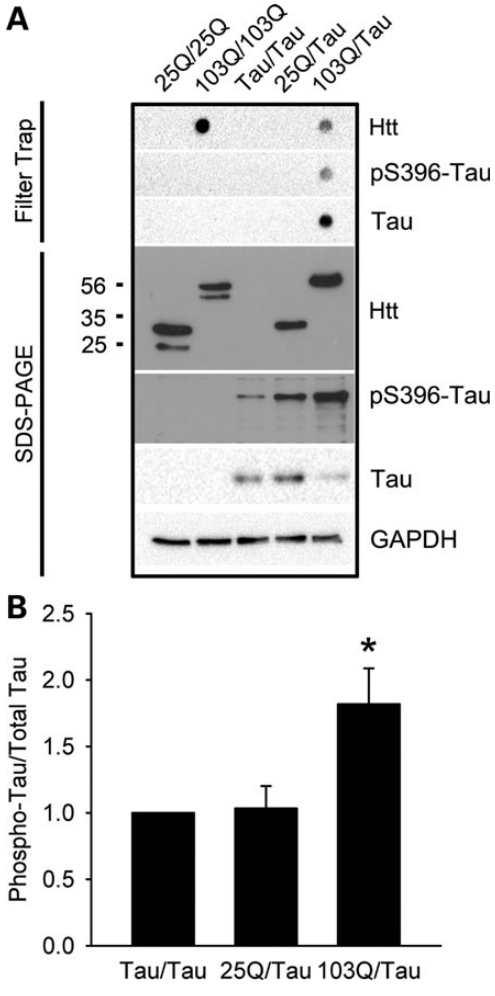

Figure 5. mHtt co-aggregates with Tau and increases the levels of Tau phosphorylation (pS396) *in vitro*. (**A**) Filter trap assays showed that mHtt, but not wild-type Htt, produced SDS-insoluble aggregates (dark dots, first line). Co-transfection of mutant Htt with Tau reduced the levels of insoluble aggregates (first line). Tau was retained in filter traps only when co-transfected with mHtt, but not wild-type Htt (second and third lines), indicating that they co-aggregate. Furthermore, retained Tau is phosphorylated at S396 (second line). SDS–PAGE immunoblots indicated that Htt/Tau co-transfection induced hyperphosphorylation of Tau at this residue (third line). Htt and GAPDH signals were used as expression and loading controls, respectively. (**B**) Quantification of Tau hyperphosphorylation see in A.

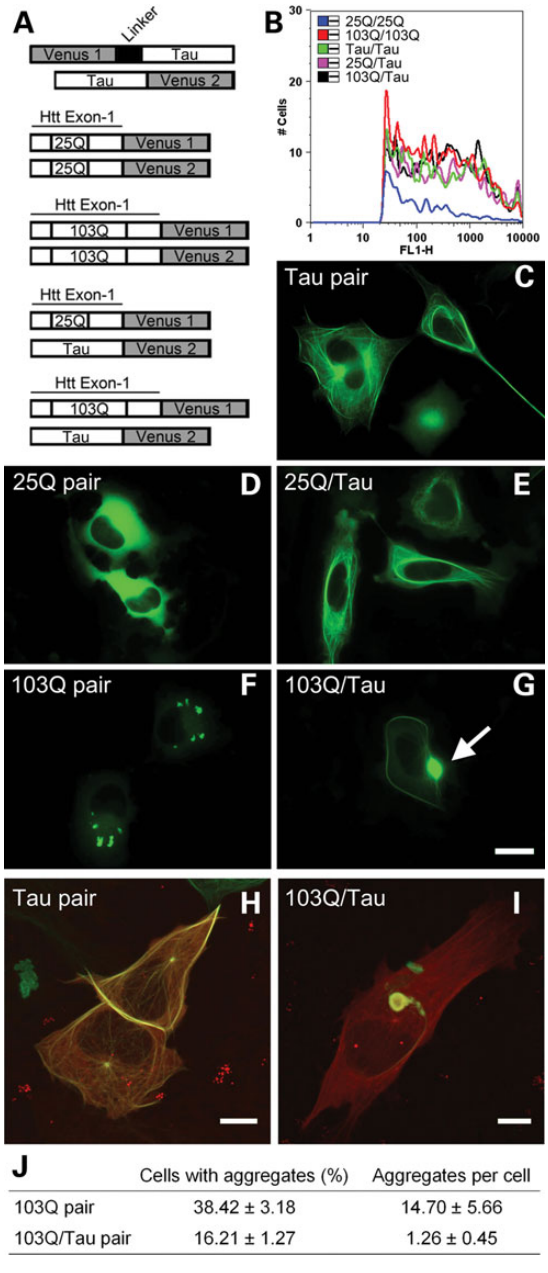

J

	Cells with aggregates (%)	Aggregates per cell
103Q pair	38.42 ± 3.18	14.70 ± 5.66
103Q/Tau pair	16.21 ± 1.27	1.26 ± 0.45

Figure 6. Mutant Htt interacts and interferes with normal Tau distribution. (**A**) Schematic of Htt- and Tau-Venus BiFC constructs. (**B**) Flow cytometry analyses of H4 cells carrying different combinations of Htt- and/or Tau-Venus BiFC constructs. (**C**–**G**) Representative pictures of the different BiFC pairs. Wild-type Htt (25Q) BiFC pairs produced most frequently a diffuse cytoplasmic fluorescence, while mutant Htt (103Q) BiFC pairs aggregated in inclusion bodies. Tau BiFC pairs showed a clearly defined microtubular localization, as expected. Combinations of 25QHtt with Tau maintained a microtubular localization, while 103QHtt disrupted Tau distribution, producing knot-like structures. No inclusion bodies are found in 103QHtt/Tau BiFC pairs. Scale bar (C–G), 20 μm. (**H** and **I**), Cells co-transfected with mCherry-Tubulin (red) and Tau/Tau or 103Q/Tau (green) pairs. Tau/Tau and 103Q/Tau dimers co-localize with the microtubular network, including MTOC, but the microtubular network of 103Q/Tau cells produced ring-like structures close to the MTOC. Co-localization of tubulin and BiFC dimers is shown in yellow. Scale bar (**H** and **I**), 5 μm. (**J**) Quantification of the frequency of cells with aggregates (percentage versus transfected cells) and the number of aggregates per cell. One hundred cells per experimental group from a total of three independent experiments were counted. Data are the average minus/plus the standard deviation.

cognitive deficits (12) and Tau loss-of-function is possibly prone to promote motor alterations in mice (35) as well as synaptic plasticity defects in the hippocampus (36), altered Tau function may underline some HD features. Whether Tau alterations precede, contribute or are concomitant to behavioral impairments and pathological features that characterize HD remains to be evaluated.

While mHtt has a clear effect on Tau phosphorylation and cellular distribution, *in vitro*, Tau also induces changes in mHtt behavior. In our cellular system, mHtt forms solid inclusions of different sizes distributed throughout the cytoplasm. These inclusions are highly dynamic, constantly recruiting new mHtt molecules to the core of the inclusion. In the presence of Tau, typical Htt aggregates almost disappear, and Htt is at least partially recruited to the microtubular network. Htt recruitment

to the microtubular network has been reported by independent laboratories (23–25). In particular, Htt is able to bind to microtubules, and has been found in the centrosome (23) and the mitotic spindle (24,25), although the biological meaning of these findings remains unclear. In a significant number of cells, one or two large ring-like inclusions are formed in the perinuclear region, where cellular quality control inclusion bodies are located. The formation of mHtt-Tau inclusions is in agreement with previous observations indicating that mHtt accumulates in cytoplasmic inclusions containing sequestrated vesicle-associated proteins, such as HSP70, dynamin or HIP1 (37). mHtt-Tau inclusions have a different morphology and are significantly less dynamic than pure mHtt inclusions or Tau dimers, indicating severe alterations in the biology of the individual proteins. Interestingly, other aggregation-prone proteins, such as transthyretin or an amyloidogenic immunoglobulin light chain, can also form ring-like inclusions (38,39). However, we are not aware of previous reports on the formation of this type of species by mHtt. Thus, our results indicate, for the first time, that at least under particular conditions, mHtt can also form this type of aggregated species. The abnormal localization/dynamics of Tau linked to its enhanced direct interaction with mHtt may also concurrently increase Tau phosphorylation. It is indeed conceivable that this interaction with mHtt would reduce the interaction of tau with its regulating phosphatase. This possibility will require further investigation in future studies.

Finally, it is noteworthy that while mHtt-induced Tau hyperphosphorylation is consistently found *in vitro* and *in vivo* using biochemical and histochemical methods, mHtt/Tau colocalization and co-aggregation is readily detected only *in vitro* using overexpression systems, but not tissue from the animal models tested. *In vitro*, under optimized conditions, co-localization was detected in ∼16% of cells. Using immunohistochemistry, we could not detect colocalization of the proteins. Since Tau hyperphosphorylation does not accumulate in mHtt-containing inclusions in mice, it is possible that the interaction between Tau and mHtt may occur before the formation of detectable/macroscopic aggregates. Together, these observations suggest that a direct mHtt/Tau interaction might be a rare phenomenon *in vivo*, and that the major impact of mHtt toward Tau is related to kinase/phosphatase imbalance.

In conclusion, our study demonstrates that mHtt expression may impact Tau functions by promoting its hyperphosphorylation. Interestingly, recent retrospective neuropathological data underlined that elderly HD demented patients exhibited AD-like lesions, supporting a relationship between mHtt and Tau (40). Moreover, another recent report demonstrated that Tau deletion improves the motor phenotype in a transgenic mouse model of HD (41). Together with our current findings, these data strongly support that Tau may play an important and understudied role in HD pathogenesis.

MATERIALS AND METHODS

In vitro experiments

Constructs and cell lines

Wild-type (25Q) and mutant (103Q) huntingtin-Venus BiFC constructs were described elsewhere (22). Tau-Venus BiFC constructs were produced by subcloning a PCR-amplified Tau gene into the Venus BiFC vectors. Tau was initially inserted in N- and C-terminal positions in order to find the combination of constructs that provides an optimal BiFC signal (22,42). Optimal Tau-Tau BiFC was obtained with a combination of constructs where Tau was located at the C-terminus of the first Venus half and the N-terminus of the second Venus half, as previously described for α-synuclein (42) (Fig. 1A). mCherry-tubulin constructs were kindly provided by Dr Domingos Henrique (Instituto de Medicina Molecular, Lisbon, Portugal).

H4 human neuroglioma cells (HTB-148, ATCC, LGC Standards, Barcelona, Spain) were maintained as described elsewhere (22,42). Cells were transfected with complementary pairs of huntingtin- and/or tau-Venus BiFC constructs using the Xtremegene reagent (Roche diagnostics, Mannheim, Germany) in a proportion 1 μg DNA: 3 μl Xtremegene. For mCherry-tubulin plus BiFC experiments (Fig. 1H and I), H4 cells were transfected first with the mCherry tubulin construct and 24 h later with the BiFC constructs. Twenty-four hours later, samples were prepared for microscopy, flow cytometry or immunoblotting and analyzed as described below.

HEK293T cells were grown in DMEM cell culture medium (Sigma-Aldrich) supplemented with 10% fetal bovine serum (Gibco) in a humidified atmosphere at 5% CO_2 at 37°C. Cells were transiently transfected 24 h after seeding with 5 μg of plasmid DNA (SIN-PGK-FLAG-htt171-82Q-myc-WHV and SIN-cPPT-PGK-human-Tau46wt-WHV), fixed 48 h after transfection with ice-cold methanol and 5 mM EGTA for 3 min, followed by permeabilization with 0.1% Triton X-100 in blocking solution (TBS, 1% bovine serum albumin) for 30 min at room temperature. Cells were then incubated with anti-c-Myc-FITC coupled (1:400, Abcam, 3G30) antibody and a Tau clone 8 antibody (AT8) (1:800, mouse, Thermo Scientific, MN1020B) with 1% bovine serum albumin in PBS at room temperature for 1 h, then incubated with Alexa Fluor 594-labeled anti-mouse IgG at room temperature for 30 min. Subsequently, cells were rinsed in TBS and treated with DAPI (Wako) diluted 1:10 000 in TBS at room temperature for 3 min and visualized by confocal microscope Leica SP8.

Flow cytometry

Cells were collected by trypsinization (5 min at 37°C), washed once with PBS and fixed in 1% (w/v) paraformaldehyde in PBS for 10 min at room temperature. Samples were analyzed by means of a FACSCalibur flow cytometer (Beckton Dickinson, Franklin Lakes, NJ, USA). Ten thousand cells were analyzed per group. Graphics and data analysis were carried out by means of the FlowJo software (Tree Star, Inc., Ahsland, OR, USA).

Fluorescence microscopy and fluorescence recovery after photobleaching experiments

Pictures were acquired from live cultures at 37°C using an Axiovert 200 M widefield fluorescence microscope or a META LSM 510 confocal microscope equipped with CCD cameras (Carl Zeiss MicroImaging GmbH, Germany). No pre-incubation at 30°C was needed, since Venus halves complement efficiently at 37°C. For fluorescence recovery after photobleaching (FRAP) experiments, protein aggregates were focused at the central focal plane and adjusted to avoid pixel saturation.

Table 1. Antibodies used in this study

Name	Abbreviation	Epitope	Type	Origin	Provider	WB
CaMKII (pThr286)	pCaMKII	pThr286	Poly	Rabbit	Cell Signaling Technology	1/1000
CaMKII	CaMKII	Human CaMKII amino-terminal region	Poly	Rabbit	Cell Signaling Technology	1/1000
Cdk5 (C-8)	Cdk5	Cdk5 COOH terminus	Poly	Rabbit	Santa Cruz Biotechnology	1/1000
Erk1/2 pThr202/Tyr204	pErk	pThr202/pTyr204	Mono	Mouse	Cell Signaling Technology	1/1000
Erk1/2 (3A7)	Erk	Mouse Erk1/2	Mono	Mouse	Cell Signaling Technology	1/1000
GAPDH	GAPDH	Human GAPDH FL 1-335	Poly	Rabbit	Santa Cruz Biotechnology	1/10 000
GAPDH	GAPDH	6C5	Mono	Mouse	Ambion	1/30 000
GSK-3β (pSer9)	pGSK3β (S9)	pSer9	Poly	Rabbit	Cell Signaling Technology	1/1000
GSK-3α/β pTyr279/Tyr216 (5G-2F)	P-GSK3β (Y216)	pTyr279/Tyr216	Mono	Mouse	Millipore	1/1000
GSK-3α/β (0011-A)	GSK3	Mouse $GSK3_{1-420}$	Mono	Mouse	Santa Cruz Biotechnology	1/2000
Huntingtin	Htt	mEM48	Mono	Mouse	Millipore	1/500
Huntingtin	Htt	2B4	Mono	Mouse	Millipore	1/500
p35 (C-19)	p35	Human P35 COOH terminus	Poly	Rabbit	Santa Cruz Biotechnology	1/1000
PP1 (E9)	PP1	Human full-length PP1	Mono	Mouse	Santa Cruz	1/1000
PP2A, C subunit, (1D6)	PP2A-C	Human PP2A C subunit 295–309	Mono	Mouse	Millipore	1/2000
PP2B (Calcineurin)	PP2B	Human Calcineurin α	Poly	Rabbit	Cell Signaling	1/1000
Tau pSer396	pSer396	pSer396	Poly	Rabbit	Invitrogen	1/10 000
Tau pSer404	pSer404	pS404	Poly	Rabbit	Invitrogen	1/10 000
Tau-1 (PC1C6)	Tau1	Non-phospho-Ser195,198,199,202	Mono	Mouse	Millipore	1/2000
Tau, Total	Cter	Cter last 15 aa of COOH terminus	Poly	Rabbit	Home-made	1/2000

Mono, monoclonal; Poly, polyclonal; WB, dilution used in western blotting.

Experiments lasted for 150 s, taking one picture every second. After five pictures to establish the basal signal, aggregates were bleached using the 488 nm laser line at 100% laser transmission on a circular region of interest with a diameter of 30 pixels (1.31 μm radius) for 5 s (10 iterations). Fluorescence recovery was then monitored for 140 s with LSM software. Data analyses were carried out on ImageJ free software (http://rsb.info.nih.gov/ij/), and represented by means of SigmaPlot 11.0 (Systat Software, Inc., Chicago, IL, USA).

Immunoblotting

Proteins were extracted in non-denaturing conditions [lysis buffer 50 mM Tris–HCl pH 7.4, 175 mM NaCl, 5 mM EDTA and a protease inhibitor cocktail tablet (Roche diagnostics, Mannheim, Germany)] as described previously (22) and quantified by the Bradford method. Twenty micrograms of protein were submitted to electrophoresis in denaturing conditions (SDS–PAGE), transferred to nitrocellulose membranes for immunoblotting. For filter trap assays, 100 mg of protein were transferred by means of a vacuum-driven dot-blot device to cellulose acetate membranes (0.2 μm pore) after addition of SDS to the samples (final concentration: 1% w/v). Membranes were washed twice with PBS plus SDS 1% (w/v) and then probed with Htt antibody as described. Only large, SDS-insoluble aggregates are retained in these membranes and, therefore, Htt signal is proportional to the amount of this type of aggregate in the samples. All antibodies used in the present manuscript are reported in Table 1. Analyses were performed using Image J Software.

Animal experiments

In the present study, we used 10-week-old R6/2 transgenic heterozygous mice overexpressing exon1 of human Huntingtin with about 120 CAG repeats and wild-type (WT) littermate controls (43). In addition, we also studied 17-month-old knock-in (KI) mice expressing chimeric mouse/human exon 1 containing 140 CAG repeats inserted in the murine huntingtin gene (KI140) and their littermate controls (44). Mice were maintained in a temperature-controlled room (~23°C) with a light/dark cycle of 12/12 h. All animals had access to food and water ad libitum. Animals were handled according to approved Animal Care procedures. Genotyping was determined from PCR of tail snips taken at 10–15 days of age. In our experiments, we used 5–6 animals per experimental group. Groups were balanced between males and females, and we did not notice gender differences regarding Tau changes as well as kinase/phosphatase modulation.

Immunoblotting

Mice were sacrificed by dislocation without anesthesia and tissue processed as described (11,12). Tissues were homogenized in 200 μl Tris buffer pH 7.4 containing 10% sucrose and protease inhibitors (Complete, Roche), sonicated and kept at −80°C for biochemical experiments. Protein dosage, processing as mono- and bi-dimensional electrophoresis, as well as sarkosyl fractionations experiments were performed as previously described (11,12).

Histological analysis

Mice brains were dissected and fixed immediately by immersion in 4% paraformaldehyde in 0.1 M phosphate buffer (pH 7.4). Samples were dehydrated in graded alcohol solutions, embedded in paraffin and cut at 5 μm using a microtome. Slices were pretreated with boiling citrate buffer, pH 6 (4 cycles of 2 min), incubated overnight in humidified chamber with anti-Htt 2B4 (mouse, 1:500, Millipore, MAB5492) or anti-Htt Em48 (mouse, 1:500, Millipore, MAB5374) and anti-Tau[pSer396] (rabbit, 1:500, Life Technologies). Samples were washed and incubated with anti-mouse IgG-Alexa Fluor 488 and anti-rabbit IgG-Alexa Fluor 594 (1:500, Life Technologies) and with DAPI,

and then subsequently washed and mounted. An inverted Leica SP8 confocal microscope was used to examine the samples.

Statistics

Results are expressed as means ± SEM. Differences between mean values were determined using the Student's *t*-test. *P*-values <0.05 were considered significant.

SUPPLEMENTARY MATERIAL

Supplementary Material is available at *HMG* online.

ACKNOWLEDGEMENTS

The authors thank the animal facility of IMPRT-IFR114 and M. Besegher, I. Brion, D. Cappe, R. Dehaynin, J. Devassine, Y. Lepage, C. Meunier and D. Taillieu for R6/2 transgenic mouse production and animal care as well as Patrizia Popoli and Alberto Martire from ISS, Roma. The authors also thank Jean-Marie Héliès and Julien Mitja (animal facility at MIRCen, CEA) for their help in developing the colony of CAG140 knock-in mice.

Conflict of Interest statement. None declared.

FUNDING

This work was supported by grants from France Alzheimer and LECMA/Alzheimer Forschung Initiative, Agence Nationale de la Recherche (ADORATAU) (D.B.). A&T laboratory is also supported by the LabEx (excellence laboratory) DISTALZ (Development of Innovative Strategies for a Transdisciplinary approach to ALZheimer's disease), Inserm, CNRS, Université Lille 2, Région Nord/Pas-de-Calais, DN2M, and FUI MEDIALZ. L.F. was the recipient of a Ph.D. fellowship from the Ministère de l'Education Nationale, de la Recherche et de la Technologie. F.H. is supported by a postdoctoral fellowship by the Portuguese Fundação para a Ciência e a Tecnologia (SFRH/BPD/63530/2009). F.H. and T.F.O. were supported by a grant from the European Huntingtoń s Disease Network (EHDN). T.F.O. was supported by an EMBO Installation Grant, and is currently supported by the DFG Center for Nanoscale Microscopy and Molecular Physiology of the Brain (CNMPB).

REFERENCES

1. Walker, F.O. (2007) Huntington's disease. *Lancet*, **369**, 218–228.
2. The Huntington's Disease Collaborative Research Group. (1993) A novel gene containing a trinucleotide repeat that is expanded and unstable on Huntington's disease chromosomes. *Cell*, **72**, 971–983.
3. Brouillet, E., Jacquard, C., Bizat, N. and Blum, D. (2005) 3-Nitropropionic acid: a mitochondrial toxin to uncover physiopathological mechanisms underlying striatal degeneration in Huntington's disease. *J. Neurochem.*, **95**, 1521–1540.
4. Sergeant, N., Bretteville, A., Hamdane, M., Caillet-Boudin, M.L., Grognet, P., Bombois, S., Blum, D., Delacourte, A., Pasquier, F., Vanmechelen, E. *et al.* (2008) Biochemistry of Tau in Alzheimer's disease and related neurological disorders. *Expert Rev. Proteomics*, **5**, 207–224.
5. Burnouf, S., Martire, A., Derisbourg, M., Laurent, C., Belarbi, K., Leboucher, A., Fernandez-Gomez, F.J., Troquier, L., Eddarkaoui, S., Grosjean, M.E. *et al.* (2013) NMDA receptor dysfunction contributes to impaired brain-derived neurotrophic factor-induced facilitation of hippocampal synaptic transmission in a Tau transgenic model. *Aging Cell*, **12**, 11–23.
6. Sultan, A., Nesslany, F., Violet, M., Begard, S., Loyens, A., Talahari, S., Mansuroglu, Z., Marzin, D., Sergeant, N., Humez, S. *et al.* (2011) Nuclear tau, a key player in neuronal DNA protection. *J. Biol. Chem.*, **286**, 4566–4575.
7. Bretteville, A. and Planel, E. (2008) Tau aggregates: toxic, inert, or protective species? *J. Alzheimers Dis.*, **14**, 431–436.
8. Planel, E., Richter, K.E., Nolan, C.E., Finley, J.E., Liu, L., Wen, Y., Krishnamurthy, P., Herman, M., Wang, L., Schachter, J.B. *et al.* (2007) Anesthesia leads to tau hyperphosphorylation through inhibition of phosphatase activity by hypothermia. *J. Neurosci.*, **27**, 3090–3097.
9. Papon, M.A., El Khoury, N.B., Marcouiller, F., Julien, C., Morin, F., Bretteville, A., Petry, F.R., Gaudreau, S., Amrani, A., Mathews, P.M. *et al.* (2013) Deregulation of protein phosphatase 2A and hyperphosphorylation of tau protein following onset of diabetes in NOD mice. *Diabetes*, **62**, 609–617.
10. Planel, E., Tatebayashi, Y., Miyasaka, T., Liu, L., Wang, L., Herman, M., Yu, W.H., Luchsinger, J.A., Wadzinski, B., Duff, K.E. and Takashima, A. (2007) Insulin dysfunction induces *in vivo* tau hyperphosphorylation through distinct mechanisms. *J. Neurosci.*, **27**, 13635–13648.
11. Leboucher, A., Laurent, C., Fernandez-Gomez, F.J., Burnouf, S., Troquier, L., Eddarkaoui, S., Demeyer, D., Caillierez, R., Zommer, N., Vallez, E. *et al.* (2013) Detrimental effects of diet-induced obesity on tau pathology are independent of insulin resistance in tau transgenic mice. *Diabetes*, **62**, 1681–1688.
12. Le Freche, H., Brouillette, J., Fernandez-Gomez, F.J., Patin, P., Caillierez, R., Zommer, N., Sergeant, N., Buee-Scherrer, V., Lebuffe, G., Blum, D. and Buee, L. (2012) Tau phosphorylation and sevoflurane anesthesia: an association to postoperative cognitive impairment. *Anesthesiology*, **116**, 779–787.
13. Eckenhoff, R.G. and Planel, E. (2013) Anesthesia, surgery and neurodegeneration. *Prog. Neuropsychopharmacol. Biol. Psychiatry*, **47**, 121.
14. Badiola, N., de Oliveira, R.M., Herrera, F., Guardia-Laguarta, C., Goncalves, S.A., Pera, M., Suarez-Calvet, M., Clarimon, J., Outeiro, T.F. and Lleo, A. (2011) Tau enhances alpha-synuclein aggregation and toxicity in cellular models of synucleinopathy. *PLoS One*, **6**, e26609.
15. Clinton, L.K., Blurton-Jones, M., Myczek, K., Trojanowski, J.Q. and LaFerla, F.M. (2010) Synergistic interactions between Abeta, tau, and alpha-synuclein: acceleration of neuropathology and cognitive decline. *J. Neurosci.*, **30**, 7281–7289.
16. Charles, V., Mezey, E., Reddy, P.H., Dehejia, A., Young, T.A., Polymeropoulos, M.H., Brownstein, M.J. and Tagle, D.A. (2000) Alpha-synuclein immunoreactivity of huntingtin polyglutamine aggregates in striatum and cortex of Huntington's disease patients and transgenic mouse models. *Neurosci. Lett.*, **289**, 29–32.
17. Furlong, R.A., Narain, Y., Rankin, J., Wyttenbach, A. and Rubinsztein, D.C. (2000) Alpha-synuclein overexpression promotes aggregation of mutant huntingtin. *Biochem. J.*, **346**, 577–581.
18. Herrera, F. and Outeiro, T.F. (2012) alpha-Synuclein modifies huntingtin aggregation in living cells. *FEBS Lett.*, **586**, 7–12.
19. Jellinger, K.A. (1998) Alzheimer-type lesions in Huntington's disease. *J. Neural Transm.*, **105**, 787–799.
20. Caparros-Lefebvre, D., Kerdraon, O., Devos, D., Dhaenens, C.M., Blum, D., Maurage, C.A., Delacourte, A. and Sablonniere, B. (2009) Association of corticobasal degeneration and Huntington's disease: can Tau aggregates protect Huntingtin toxicity? *Mov. Disord.*, **24**, 1089–1090.
21. Tian, Q. and Wang, J. (2002) Role of serine/threonine protein phosphatase in Alzheimer's disease. *Neurosignals*, **11**, 262–269.
22. Herrera, F., Tenreiro, S., Miller-Fleming, L. and Outeiro, T.F. (2011) Visualization of cell-to-cell transmission of mutant huntingtin oligomers. *PLoS Curr.*, **3**, RRN1210.
23. Hoffner, G., Kahlem, P. and Djian, P. (2002) Perinuclear localization of huntingtin as a consequence of its binding to microtubules through an interaction with beta-tubulin: relevance to Huntington's disease. *J. Cell Sci.*, **115**, 941–948.
24. Godin, J.D., Colombo, K., Molina-Calavita, M., Keryer, G., Zala, D., Charrin, B.C., Dietrich, P., Volvert, M.L., Guillemot, F., Dragatsis, I. *et al.* (2010) Huntingtin is required for mitotic spindle orientation and mammalian neurogenesis. *Neuron*, **67**, 392–406.

25. Atwal, R.S., Desmond, C.R., Caron, N., Maiuri, T., Xia, J., Sipione, S. and Truant, R. (2011) Kinase inhibitors modulate huntingtin cell localization and toxicity. *Nat. Chem. Biol.*, **7**, 453–460.
26. Torres-Peraza, J.F., Giralt, A., García-Martínez, J.M., Pedrosa, E., Canals, J.M. and Alberch, J. (2008) Disruption of striatal glutamatergic transmission induced by mutant huntingtin involves remodeling of both postsynaptic density and NMDA receptor signaling. *Neurobiol. Dis.*, **29**, 409–421.
27. Hodges, A., Strand, A.D., Aragaki, A.K., Kuhn, A., Sengstag, T., Hughes, G., Elliston, L.A., Hartog, C., Goldstein, D.R., Thu, D. *et al.* (2006) Regional and cellular gene expression changes in human Huntington's disease brain. *Hum. Mol. Genet.*, **15**, 965–977.
28. Xifro, X., Giralt, A., Saavedra, A., Garcia-Martinez, J.M., Diaz-Hernandez, M., Lucas, J.J., Alberch, J. and Perez-Navarro, E. (2009) Reduced calcineurin protein levels and activity in exon-1 mouse models of Huntington's disease: role in excitotoxicity. *Neurobiol. Dis.*, **36**, 461–469.
29. Luthi-Carter, R., Strand, A., Peters, N.L., Solano, S.M., Hollingsworth, Z.R., Menon, A.S., Frey, A.S., Spektor, B.S., Penney, E.B., Schilling, G. *et al.* (2000) Decreased expression of striatal signaling genes in a mouse model of Huntington's disease. *Hum. Mol. Genet.*, **9**, 1259–1271.
30. Hernandez-Espinosa, D. and Morton, A.J. (2006) Calcineurin inhibitors cause an acceleration of the neurological phenotype in a mouse transgenic for the human Huntington's disease mutation. *Brain Res. Bull.*, **69**, 669–679.
31. Liu, F., Grundke-Iqbal, I., Iqbal, K. and Gong, C.X. (2005) Contributions of protein phosphatases PP1, PP2A, PP2B and PP5 to the regulation of tau phosphorylation. *Eur. J. Neurosci.*, **22**, 1942–1950.
32. Jenkins, S.M., Zinnerman, M., Garner, C. and Johnson, G.V. (2000) Modulation of tau phosphorylation and intracellular localization by cellular stress. *Biochem. J.*, **345**, 263–270.
33. Buee, L., Bussiere, T., Buee-Scherrer, V., Delacourte, A. and Hof, P.R. (2000) Tau protein isoforms, phosphorylation and role in neurodegenerative disorders. *Brain Res. Brain Res. Rev.*, **33**, 95–130.
34. Hinckelmann, M.V., Zala, D. and Saudou, F. (2013) Releasing the brake: restoring fast axonal transport in neurodegenerative disorders. *Trends Cell Biol.*, **23**, 634–643.
35. Morris, M., Maeda, S., Vossel, K. and Mucke, L. (2011) The many faces of tau. *Neuron*, **70**, 410–426.
36. Ahmed, T., Van der Jeugd, A., Blum, D., Galas, M.C., D'Hooge, R., Buee, L. and Balschun, D. (2014) Cognition and hippocampal synaptic plasticity in mice with a homozygous tau deletion *Neurobiol. Aging* (in press). doi: 10.1016/j.neurobiolaging.2014.05.005.
37. Qin, Z.H., Wang, Y., Sapp, E., Cuiffo, B., Wanker, E., Hayden, M.R., Kegel, K.B., Aronin, N. and DiFiglia, M. (2004) Huntingtin bodies sequester vesicle-associated proteins by a polyproline-dependent interaction. *J. Neurosci.*, **24**, 269–281.
38. Pires, R.H., Karsai, Á., Saraiva, M.J., Damas, A.M. and Kellermayer, M.S. (2012) Distinct annular oligomers captured along the assembly and disassembly pathways of transthyretin amyloid protofibrils. *PLoS One*, **7**, e44992.
39. Zhu, M., Han, S., Zhou, F., Carter, S.A. and Fink, A.L. (2004) Annular oligomeric amyloid intermediates observed by *in situ* atomic force microscopy. *J. Biol. Chem.*, **279**, 24452–24459.
40. Davis, M.Y., Keene, C.D., Jayadev, S. and Bird, T. (2014) The co-occurrence of Alzheimer's disease and Huntington's disease: a neuropathological study of 15 elderly Huntington's disease subjects. *J. Huntingtons Dis.*, **3**, 209–217.
41. Fernández-Nogales, M., Cabrera, J.R., Santos-Galindo, M., Hoozemans, J.J., Ferrer, I., Rozemuller, A.J., Hernández, F., Avila, J. and Lucas, J.J. (2014) Huntington's disease is a four-repeat tauopathy with tau nuclear rods. *Nat. Med.*, **20**, 881–885.
42. Outeiro, T.F., Putcha, P., Tetzlaff, J.E., Spoelgen, R., Koker, M., Carvalho, F., Hyman, B.T. and McLean, P.J. (2008) Formation of toxic oligomeric alpha-synuclein species in living cells. *PLoS One*, **3**, e1867.
43. Mangiarini, L., Sathasivam, K., Seller, M., Cozens, B., Harper, A., Hetherington, C., Lawton, M., Trottier, Y., Lehrach, H., Davies, S.W. *et al.* (1996) Exon 1 of the HD gene with an expanded CAG repeat is sufficient to cause a progressive neurological phenotype in transgenic mice. *Cell*, **87**, 493–506.
44. Menalled, L.B., Sison, J.D., Dragatsis, I., Zeitlin, S. and Chesselet, M.F. (2003) Time course of early motor and neuropathological anomalies in a knock-in mouse model of Huntington's disease with 140 CAG repeats. *J. Comp. Neurol.*, **465**, 11–26.